Experimental validation of the plunger-type flow model for irregular waves

Stephanie Lowell, Rishad A. Irani

Multi-Domain Laboratory, Carleton University, 1125 Colonel By Dr., Ottawa, Ontario, Canada

Abstract

In this paper, a study of irregular waves generated with a plunger-type wavemaker with the inclusion of mean flow is conducted along with an analysis of the standard plunger-type flow (PTF) model. It was determined that for high frequencies, the standard PTF model exhibits amplification which when compared to theoretical models for piston- and flap-type wavemakers is implausible. Therefore, a correction to the PTF model has been proposed for use with irregular waves that limits the value of the wave amplitude a to stroke amplitude s ratio a/s to one or less. Experimental validation of the correction is also given along with a study on the performance of the plunger system for generating the desired irregular Bretschneider wave spectrum. In this paper, multiple significant wave heights and peak frequencies are considered for no-flow and three mean flow cases. The experimental results showed that not only is the proposed correction valid for decreasing the percent error in the significant wave height but, plunger-type wavemakers are capable of accurately producing irregular spectra regardless of the inclusion of mean flow.

Keywords: Wave generation, plunger-type wavemaker, mean flow, irregular waves, water channel, Bretschneider spectrum

1. Introduction

The sea surface is known to be highly irregular and random under a variety of conditions; thus, the energy associated with ocean waves are a natural phenomena that can be a challenge to predict. Since wave energy can be transferred to a sea-going vessel, it is important to understand how the energy is distributed and to properly model the energy for a set of waves. As such, the interaction between sea waves and ships as well as the coupling effects of waves is a prominent research topic [1, 2, 3]. Laboratory water channels provide an indispensable environment for modelling and understanding the fundamental energy models of such ocean interactions. By scaling the ocean environment to the laboratory scale, applications often performed in irregular sea waves can be studied in a controlled environment, such as launch and recovery operations

[4] and tow-body dynamics [5, 6]. Irregular waves can be generated in a water channel through the use of a wavemaker, the three commons types of which include piston-, flap-, and plunger-type [7]. While many of these wavemaker systems have been used to generate irregular waves in a water channel, the experimental work rarely considers the effect of mean flow on the produced wave spectra. Recently, an analytical model representing the transfer function for plunger-type wavemakers was extended to include mean flow [8]. Due to the inclusion of mean flow, the model was deemed the plunger-type flow (PTF) model; however, experimental work only considered the generation of regular waves. Therefore, as an extension to the work conducted in [8], this paper aims to explore the implementation of irregular waves using the PTF model with experimental validation. In addition, the shortcomings of the PTF model for high frequencies will be identified with a proposed correction.

The most commonly used wavemakers for generating irregular waves are those of the piston- and flap-type wavemakers, owing to the well established theoretical models and experimental work governing their performance. Miskovic et al. [9] used a piston-type wavemaker to implement a system for generating irregular waves for the purpose of testing sea wave impact on coastal facilities. To model coastal wave dynamics, Raoult et al. [10] developed a non-linear potential flow model for a piston-type wavemaker using a spectral method and the time evolution of the free surface position and free surface velocity potential. Simulation of the model was validated using experimental data with respect to both regular and irregular waves, but the model was specific to piston-type wavemakers and did not include the effects of mean flow within the channel. Riefolo et al. [11] made use of a flap-type wavemaker in a laboratory water channel to experimentally study the effects of wave grouping and long-wave short-wave combination regimes on low frequency generations. Khait and Shemer [12] also used a flap-type wavemaker to explore the generation of steep regular and irregular waves using non-linear water wave models. Other research has focused more specifically on the wave spectra generated within the water channel. Xu et al. [13] investigated two new wave spectra, a quasi constant wave amplitude spectrum and a quasi constant wave steepness spectrum. The work utilized a flap-type wavemaker to experimentally investigate the results of generating space-time focusing waves based on the spectra. More recently, Guler et al. [14] used a piston-type wavemaker to generate JONSWAP spectra to study the cross-shore distribution of non-buoyant microplastic particles for irregular waves propagating, shoaling, and breaking on live sediment sloping beds. While the use of piston- and flap-type wavemakers is common, their design within a water channel does not typically allow for mean flow across the lateral boundary. The inclusion and impact of mean flow is important in order to further understand the energy profile that is generated in a full-scaled ocean environment. Thus, plunger-type wavemakers are advantageous as their design allows for mean flow to move across the lateral boundary while simultaneously generating waves without the need to submerge any mechanical parts.

The use of plunger-type wavemakers is becoming increasingly popular in research with research focusing on both analytical and numerical solutions for de-

scribing the transfer function between the wavemaker and the generated waves. However, there is still a deficit in knowledge on the plunger system's performance as compared to piston- and flap-type wavemakers. Regardless, plunger-type wavemakers have been shown to be able to generate irregular waves. Recently, Hasnan et al. [15] used a plunger-type wavemaker in a large water channel in order to study the turning behaviour of ships in irregular waves. However, the accuracy of the plunger system to produce the desired irregular wave profile was limited to a single spectrum and the experimental work did not include mean flow. Sun et al. [16] studied a variety of waves using a numerical simulation and compared it to the results of an analytical method based on mass conservation. The study considered the generation of irregular waves as well as regular waves, solitary waves, and Stokes fifth order waves; however, no experimental work was conducted and mean flow was neglected.

Early use of plunger-type wavemakers began with cylindrical shaped wedges, the theory of which developed by Ursell [17, 18], who considered an infinite water depth to determine the prescribed wave amplitude being produced. Yu and Ursell [19] validated the theory through experimental work. Wang [20] used a two parameter conformal transformation to develop theoretical curves for different size triangular-shaped plunger systems. While experimental work was conducted to validate the theoretical model, the model also assumed infinite water depth. To extend the general wavemaker theory presented by Biesel [21], Hyun [22] applied potential flow theory to a triangular shaped wedge, taking into consideration and studying the total hydrodynamic force on the wedge. Ellix and Arumugam [23] studied the wave profile generated by a plunger system in a water channel and found their overall waveform consisted of a second order Stokes wave, a free second harmonic wave, and reflected components at both the fundamental and second harmonic frequencies. A non-linear numerical method was presented by Kashiwagi [24] for a wedge-shaped wavemaker, whose results of producing regular waves were found to be in agreement with linear models and experimental findings. Mikkola [25, 26] studied the performance of wedges with different inner angles with respect to the generated wave height and wave quality of regular waves as part of a wavemaker renewal project. The results of the work showed that the motion frequency has a significant influence on the wave quality and that a larger angle resulted in waves with larger amplitudes. However, the work did not take into consideration the increased submerged volume with the larger angles nor did the experimental work include mean flow. More recently, He et al. [27] investigated a plunger-type wavemaker's ability to generate solitary waves, considering wedge-shaped, box-shaped, and cylindrical-shaped plungers. Using a Smoothed Particle Hydrodynamics model, their simulation showed that in comparison to piston-type wavemakers, the solitary wave generated by a plunger-type wavemaker can be just as accurate.

One analytical method that has been of particular interest is that of the work published by Wu [28]. The work proposed a semi-analytical method using potential flow theory to develop the transfer function between the wave amplitude a and the stroke amplitude of the plunger s. The amplitude ratio a/s incorporated the water depth into the final model as an extension to Wang's [20] work

with the plunger-type system. Many experimental and numerical work has been conducted since, using the model and results of [28] as a baseline. Wu [29] themselves compared a new method using the Boundary Element Method to their previous work along with a comparison to the experimental work conducted in [23]. Gadelho et al. [30] made reference to the analytical work in [28] when constructing a plunger-type wavemaker for a laboratory water channel. The work included both an experimental analysis and a numerical model which were in good agreement. To address the shortcomings in [25, 26], Azadian-Kharanjani et al. [31] used a numerical method to investigate the effects of wedge angle for plunger-type wavemakers with a constant submerged volume. The simulation results were directly compared to results generated with the models presented by Wang [20] and Wu [28], explicitly showing the associated a/s curve as a function of the dimensionless parameter kb where k is the wavenumber and b is the width of the wedge. It was found that in deep water, the wedge angle has no significant effect on the quality of the generated wave. Nikseresht and Bingham [32] also used numerical methods to investigate the performance of plunger-shaped wavemakers. Their work focused on modelling and understanding the two-dimensional gap and shape effects of the plunger system generating regular waves, whose back is aligned with one end of the water channel. The results of investigation used the linear theory in [28] as a baseline for validation of the simulation, providing the a/s curve as a function of angular frequency and the dimensionless parameter kb. A sensitivity analysis of the model in [28] was performed by Lowell et al. [33], who also introduced and studied the inclusion of mean flow as an input parameter to the model. The results of the sensitivity analysis showed that individually frequency is the most influential parameter in the model and that mean flow is not as influential; however, the inclusion of mean flow is important due to the interactions between parameters. Hicks et al. [34] developed a non-linear model for generating regular waves with a plunger system with direct comparison to the model in [28] and validation with experimental data. The research investigates and aims to optimize the controls signals required to move a wedge-shape system, demonstrating both the applicability and suitability of the procedure. As an extension to the work in [33], Lowell et al. [8] provided an extensive experimental analysis of a plunger-type wavemaker system which included the effects of mean flow. The new model, named the plunger-type flow (PTF) model, was proposed and experimentally validated for regular waves. It was found that to more accurately predict the generated waves, an operational correction was required which worked to decrease the theoretical a/s of the PTF model by 26% regardless of the input parameters. Boon and Wellens [35] referenced the PTF model in their experimental setup for collecting green water data in sea states. In their work, a plunger-type wavemaker was used to create irregular waves with mean flow, focusing on quantifying the probability of occurrence of green water and the expected maximum pressures on a laboratory scaled ship. However, the experimental work did not address the accuracy of the desired spectra or the impact of mean flow on the experimental data as the variation in mean flow was negligible.

In the original work by Wu [28] and in some of the research that followed it

[31, 32, 34], explicit figures of the linear model as a function of dimensionless parameter kb were provided, which is proportional to the frequency. Such figures show that as the frequency increases, a/s can have a value greater than one, meaning that amplification of the wave amplitude can occur for a given stroke. However, no discussion is given to explain the phenomenon nor does the research explore the behaviour of the model for higher frequencies. Since a wide range of frequencies are required in order to create irregular wave spectra, the inclusion of high frequency bands is important. The central aim of the paper therefore seeks to show the behaviour for a wider range of frequencies of the PTF model, and thereby the Wu model [28], and correct the model with respect to the observed amplification. The specific contributions are:

1. A proposed correction to the PTF model which eliminates the observed theoretical wave amplification phenomena,
2. Validation of the proposed correction using experimental data of irregular waves generated using the uncorrected and corrected PTF model,
3. Experimental investigation on the impact of mean flow when generating a desired wave spectra using a plunger-type wavemaker.

The study of mean flow on irregular wave spectra will contribute further understanding to the energy in real ocean environments while establishing the effect of mean flow will be useful for future hydrodynamic applications in a laboratory water channel. Note that the proposed correction in this paper differs from the operational correction in [8] in that the proposal applies to all frequencies for a given set of parameters whereas the previous correction only applied to a single frequency for a given set of parameters.

Section 2 outlines the theory governing irregular waves and common wave spectra. Section 3 describes the experimental setup of the plunger-type system along with a proposed correction to the model while Section 4 outlines the experimental design. The results of the experimental work are included in Section 5 with concluding remarks given in Section 6.

2. Irregular Waves

The general condition of the free surface of the ocean at any given time and location can be described by its sea state, the definition of which is not unique. The North Atlantic Treaty Organization (NATO) and the World Meteorological Organization (WMO) [36] define each sea state by the model period T_p which corresponds to the peak frequency of the wave energy density spectrum and the significant wave H_s. In the time-domain, the significant wave height H_s is mathematically expressed as,

$$H_s = \frac{1}{N_H/3} \sum_{i=1}^{N_H/3} H_i, \tag{1}$$

where N_H is the total number of individual wave heights, and H_i is a series of wave heights ranked from highest to lowest. Table 1 outlines the parameters that describe sea states 2-6 as defined by the NATO/WMO code [36].

Table 1: Sea state definition by NATO STANAG 4194 Annex D [36].

Sea State	Significant Wave Height [m]		Modal Period [s]	
	Range	Mean	Range	Most Probable
2	0.1-0.5	0.30	3.3-12.8	7.5
3	0.5-1.25	0.88	5.0-14.8	7.5
4	1.25-2.5	1.88	6.1-15.2	8.8
5	2.5-4.0	3.75	8.3-15.5	9.7
6	4.0-6.0	5.00	9.8-16.2	12.4

A specific sea state can be adequately represented by a series of different regular waves of varying heights, lengths, and phases that are superimposed on each other. Thus, ocean waves are most conveniently described by their energy density spectra $S(\omega)$. A number of empirical spectrum formula exist for describing the sea surface, each of which being site-specific. The most commonly used spectra are the Pierson-Moskowitz (P-M), the JONSWAP, and the Bretschneider. The P-M spectrum assumes a fully developed sea, such that winds blowing steadily for a long time over a large area have created waves that are in equilibrium with the wind [37]. On the other hand, the Joint North Sea Wave Observation Project (JONSWAP), found that the wave spectrum is never fully developed, instead it continues to develop through non-linear, wave-wave interactions even for very long times and distances [37]. Thus, the JONSWAP spectrum is often used for fetch-limited conditions in coastal waters and when seas are fully developed, reduces to the P-M spectrum. Finally, the Bretschneider spectrum is the standard for open-ocean conditions as it does not require seas to be fully developed [38]. For the same amount of energy, the P-M, JONSWAP, and Bretschneider spectra each distribute the energy differently across the frequency band. Therefore, the theoretical surface of the ocean will be dependent on the spectrum model applied. Due to its wide applicability and the simplicity of the empirical formula, the Bretschneider spectrum will be used for developing irregular wave profiles to be reproduced in the water channel in this study.

The Bretschneider spectrum is a two parameter spectrum based on the peak frequency ω_0 and significant wave height H_s. Defined as a function of angular frequency ω, the Bretschneider spectrum $S_B(\omega)$ is mathematically expressed as,

$$S_B(\omega) = \frac{1.25}{4}\frac{\omega_0^4}{\omega^5}H_s^2 \exp\left[-1.25\left(\frac{\omega_0}{\omega}\right)^4\right], \tag{2}$$

where ω_0 and H_s are specified independently from one another [39]. Figure 1 plots the energy density spectrum as a function of the wave frequency to demonstrate the differences in the Bretschneider spectrum for the mean significant wave heights corresponding to sea states 2-6 in Table 1 with $\omega_0 = 0.2\pi$ ($T_p = 10$s). For the same input peak frequency, the spectrum energy and significant wave height are quadratically proportional to each other such that an increase in significant wave height will lead to an increase in wave energy and vice versa.

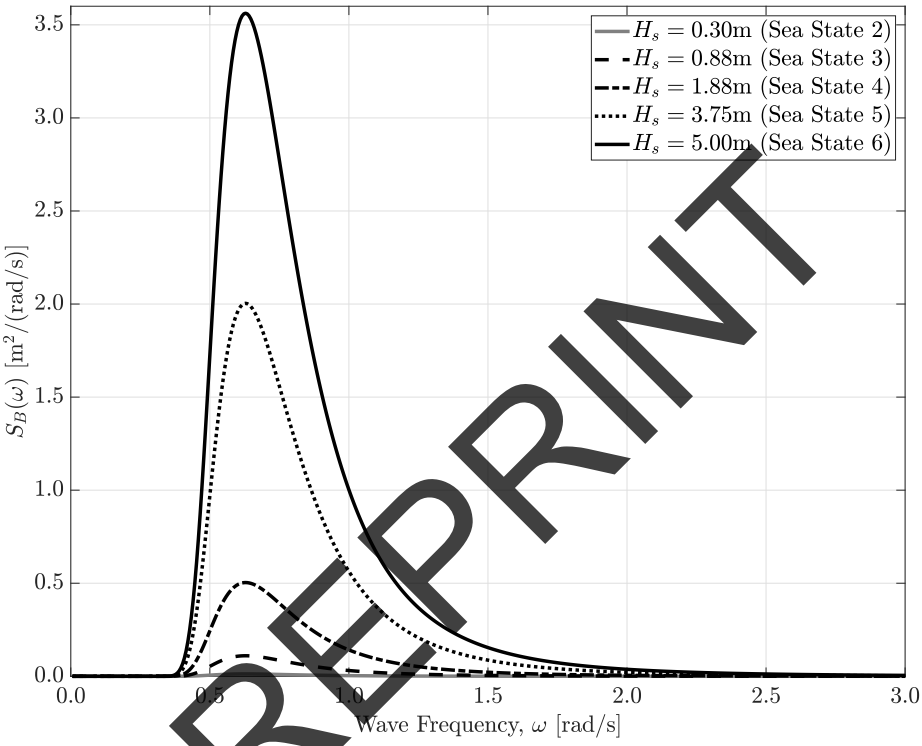

Figure 1: Various energy spectrum densities governed by the Bretschneider spectrum. Here, $\omega_0 = 0.2\pi$ for the mean significant wave heights of sea states 2-6.

Irregular waves can be generated in a water channel based on a desired wave spectrum model. However, for a time-domain analysis, such as the one required for the plunger-type wavemaker system used herein, the time history of the ocean must be computed from the wave spectrum [40]. For convenience, the Bretschneider spectrum may be initially rewritten as a function of frequency f instead of the angular frequency ω such that,

$$S_B(f) = \frac{1.25}{8\pi}\frac{f_0^4}{f^5}H_s^2 \exp\left[-1.25\left(\frac{f_0}{f}\right)^4\right]. \tag{3}$$

The desired energy density spectrum is discretized into N_f equidistant frequency bands with width Δf. Each frequency band represents the amplitude of one harmonic in the resulting time-domain signal where the phase for each harmonic is chosen at random. Thus, the surface elevation in the time-domain $\eta(t)$ is calculated using Fourier analysis as a sum of the individual harmonics,

$$\eta(t) = \sum_{f=f_1}^{f_{N_f}} \sqrt{2S_B(f)\Delta f}\cos(2\pi f t + \varphi(f)), \tag{4}$$

where f_1 corresponds to the average frequency of the first Δf band up to the $N_f - th$ band and $\varphi(f)$ is the random phase offset [39, 40]. The wave height is then derived from the coefficient of the surface elevation in Eq. (4),

$$H(f) = 2\sqrt{2S_B(f)\Delta f}. \tag{5}$$

For practical applications in a water channel, there exists a transfer function between the surface elevation and the control signal of the wavemaker. In the time-domain, the transfer function is generally dependent on a single frequency f. Thus, for irregular waves, which are comprised of a range of frequencies, the control signal must initially be determined in the frequency-domain. To do so, the transfer function is applied to the amplitude spectrum of the desired wave profile, resulting in an amplitude spectrum representative of the control signal. The wavemaker control signal in the time-domain $z(t)$ can be described similar to the surface elevation in Eq. (4) such that,

$$z(t) = \sum_{f=f_1}^{f_{N_f}} \sqrt{2S_s(f)\Delta f}\cos(2\pi f t + \varphi(f)), \tag{6}$$

where $S_s(f)$ is the wavemaker control signal in the frequency-domain. Therefore, using Eq. (6), control signals corresponding to various Bretschneider spectra can be developed for experimental testing in a laboratory setting with a plunger-type wavemaker and its associated transfer function.

3. The Plunger-type Wavemaker

The experimental system studied in this paper consists of a plunger-type wavemaker with a triangular cross-section. Fig. 2 provides a schematic diagram of the water channel outlining its important features. Waves are generated by oscillating the wedge along the z-axis with the corresponding wave amplitude represented by a at a known still water depth h. The wavemaker is located at the end of the contraction section such that waves propagate through the test section and towards the end of the channel (discharge section). The mean water flow U is circulated through the channel along the positive x-direction such that in this paper, only waves-with-flow are considered. Note that "mean flow" refers to when an applied flow is included in the water channel; whereas,

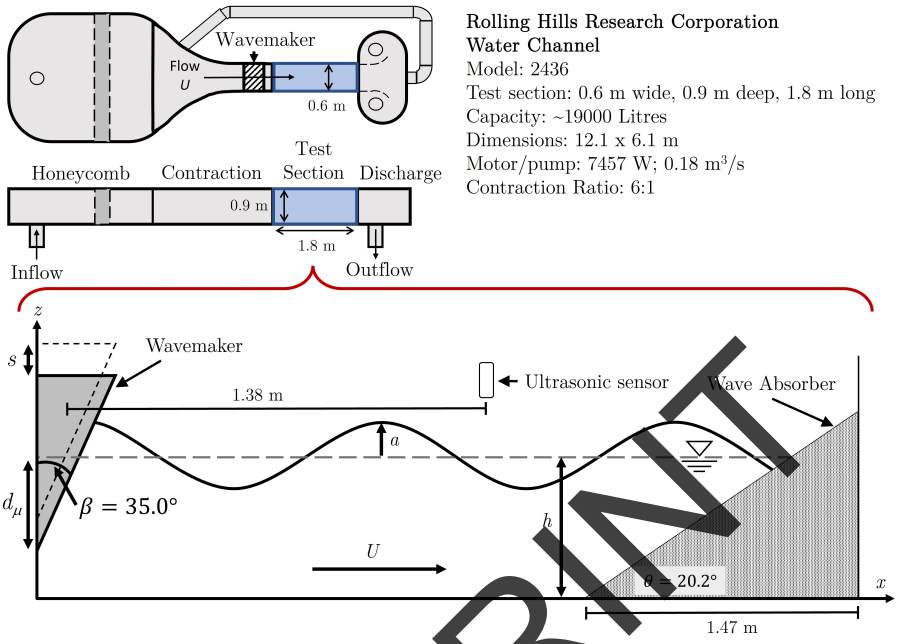

Figure 2: Schematic of the water channel including location of the plunger-type wavemaker and dimensions of the test section through which the waves propagate. Also shown is the ultrasonic sensor and wave absorber, along with the direction of mean flow U.

"no-flow" will refer to the absence of an applied flow. The end of the channel is also configured such that flow angularity and turbulence is not developed and propagated upstream. It was determined that a wedge with an inner angle of $\beta = 35.0°$ is able to generate the most stable and accurately predicted waves regardless of mean flow [8]. The stroke of the wavemaker is represented by s while the mean depth with respect to the still water line is given by d_μ.

Downstream of the wedge, an ultrasonic sensor produced by SICK is positioned above the channel in order to measure the surface elevation [41]. Compared to traditionally used wave gauges, the ultrasonic sensor produces comparable results with the advantage of being a non-contact method of surface elevation measurement [42]. Furthermore, the water channel is equipped with a wave absorber in order to reduce any reflected wave energy from the end of the channel. The wave absorber used herein consists of a sloped, perforated board which aids in the dissipation of incident waves generated by the wavemaker as they pass through the board. Regardless, there will still exist some reflected wave energy which may propagate upstream and interfere with the generated wave spectrum. To further reduce the reflected energy, the board is also equipped with rope which acts in a similar manner to the way sea grass attenuates wave energy in coastal regions. As a result, for the experimental set-up shown in Fig. 2, the ratio of incident wave height to reflected wave height,

also referred to as the reflection coefficient, is 0.36 [33].

Photographs of the water channel set-up are provided in Fig. 3, which highlights the location of the wavemaker, ultrasonic sensor, and wave absorber from multiple points of view. While the test section on traditional water channels

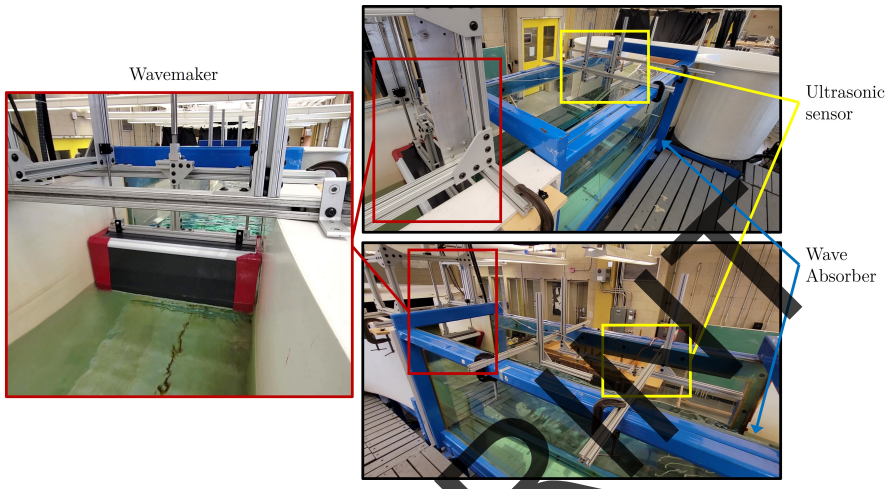

Figure 3: Photographs of the laboratory water channel showing the plunger-type wavemaker, ultrasonic sensor, and wave absorber.

are often longer, the water channel used herein was not originally designed in consideration of wave generation. As such, the length of the test section for generating waves is limited. In the plunger-type wavemaker theory developed by Wu [28], a semi-infinite channel was assumed such that standing waves will decay exponentially with distance from the wavemaker, leaving only progressive waves in the far-field. For the finite length of the channel used herein, analysis of the dispersion relation concludes that standing waves will be negligible compared to the progressive waves at a distance fo $2h$ from the wavemaker [40, 43]. Thus, to ensure that fully developed, progressive waves are measured in the channel, the ultrasonic was placed 1.38 m from the centre of the wavemaker, as displayed in Fig. 2, while the water depth was set to 0.60 m.

The transfer function a/s between the stroke amplitude s of the wedge and the generated wave amplitude a is described by the PTF model,

$$a/s = \left| -i_m A_1' k_p h \sinh(k_p h) \right|, \tag{7}$$

where i_m is the imaginary number, and k_p is the progressive wavenumber [8]. The coefficient A_1' is determined using Wu's [28] boundary collocation method based on potential flow theory. By modifying the dispersion relation governing the desired wave profile, a mean flow U is also included in the model, a detailed derivation of which is available in [8, 33].

3.1. Correction to the PTF Model

Along with plunger-type wavemakers, piston- and flap-type wavemakers are also used in laboratory water channels. Unlike the plunger system through, piston and flap wavemakers require some mechanical parts to be submerged in the water. As such, it usually requires the wavemaker to be installed during construction of the channel rather than as a post-build addition. The transfer functions for piston- and flap-types are well established with research and experimental work on both reaching maturity. That being said, they do provide a framework for which to compare the plunger system. The transfer function for piston-type a/s_p and flap-type a/s_f wavemakers is given respectively by,

$$a/s_p = \frac{\cosh(2kh) - 1}{\sinh(2kh) + 2kh}, \tag{8}$$

$$a/s_f = \frac{2\sinh(kh)}{kh} \frac{kh\sinh(kh) - \cosh(kh) + 1}{\sinh(2kh) + 2kh}, \tag{9}$$

where k is the wavenumber [40]. Fig. 4 plots the transfer function for the three wavemaker types as a function of frequency as given (top) and with proposed corrections (bottom). While the frequency, and accordingly the wavenumber k, is varied, the remaining input parameters for each wavemaker transfer function were equal and held constant regardless of wavemaker type such that $h = 0.60$ m, $\beta = 35.0°$, $d_\mu = 0.12$ m, and $U = 0$ m/s. In Fig. 4 (top) the piston (blue) and flap (green) type wavemaker transfer functions saturate at one as the frequency increases; however, the plunger-type transfer function (red) exhibits a peak that extends beyond $a/s = 1$ before decreasing to a value below one at the higher frequencies. It is also noted that due to the nature of the hyperbolic sine function (sinh) terms in each of the transfer functions, an asymptote is observed that effectively sets the value of a/s to NaN (Not a Number) for frequencies beyond a limit. The exact value of such limit is governed by the chosen input parameters; for the example in Fig. 4 (top) the limit is approximately 12 Hz.

A value of a/s greater than one suggests that the amplitude of generated waves is greater than that of the stroke amplitude which theoretically would require the wave to gain more energy than what is provided to it by the wavemaker. A similar trend is observed regardless of the wedge angle, mean wedge depth, water depth, and mean flow. Since such an increase in energy is not theoretically plausible, a fact that is reinstated by the saturation of the piston- and flap-type transfer functions at one, the authors' propose that a correction is required to the PTF model to alleviate the amplification issue. Fig. 4 (bottom) displays the proposed correction to the plunger-type transfer function which applies a bias to a/s such that the local maximum reduces to one and a/s is then saturated for all higher frequencies. Mathematically, the bias is applied by dividing a/s at each frequency by the maximum value of a/s. For notation purposes, the ratio a/s will be represented by α such that the corrected ratio

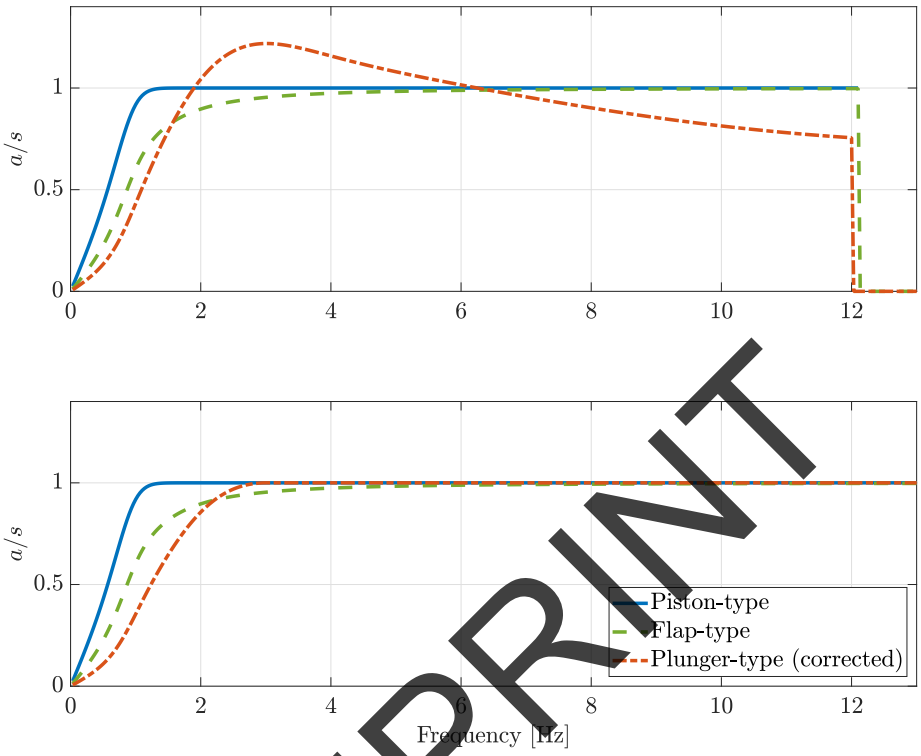

Figure 4: The a/s ratio for the piston-, flap-, and plunger-type wavemakers as a function of frequency. The top panel shows the models as given whereas the bottom panel shows the models with the appropriately applied corrections.

$\alpha_c(f)$ is determined by,

$$\alpha_c(f) = \frac{\alpha(f)}{\max(\alpha)}, \tag{10}$$

where $\alpha(f)$ represents the wave amplitude to stroke amplitude ratio as a function of frequency f and $\max(\alpha)$ is the maximum value. The frequency at which the maximum value of α occurs, and therefore the bias, will be dependent on the input parameters to the PTF model. Thus, the input parameters must be known prior to experimental testing in order to apply the appropriate correction. After applying the bias, the saturation of the PTF model is then represented by,

$$\alpha_c(f) = \begin{cases} \alpha_c, & f < f(\max(\alpha_c)), \\ 1, & f \geq f(\max(\alpha_c)), \end{cases} \tag{11}$$

such that the curve is of class C^0 in that it is continuous but not differentiable. In applying the saturation to all values of α_c for frequencies greater than the maximum α_c frequency, the discontinuity due to the hyperbolic sine term in

the PTF model in Eq. (7), exemplified at $f = 12$ Hz in Fig. 4 (top), is effectively removed. Fig. 4 (top) also shows that the piston- and flap-type transfer functions, Eq. (8) and Eq. (9), respectively, also experience a discontinuity due to the hyperbolic sine terms in their respective equations. It is assumed that in literature, the piston- and flap-type transfer functions are accordingly saturated, using a function such as Eq. (11) to avoid the discontinuity at higher frequencies which has also been reflected in Fig. 4 (bottom).

Fig. 5 shows the impact of proposed PTF model correction on the stroke amplitude spectrum $S_a(f)$. An example Bretschneider wave amplitude spectrum

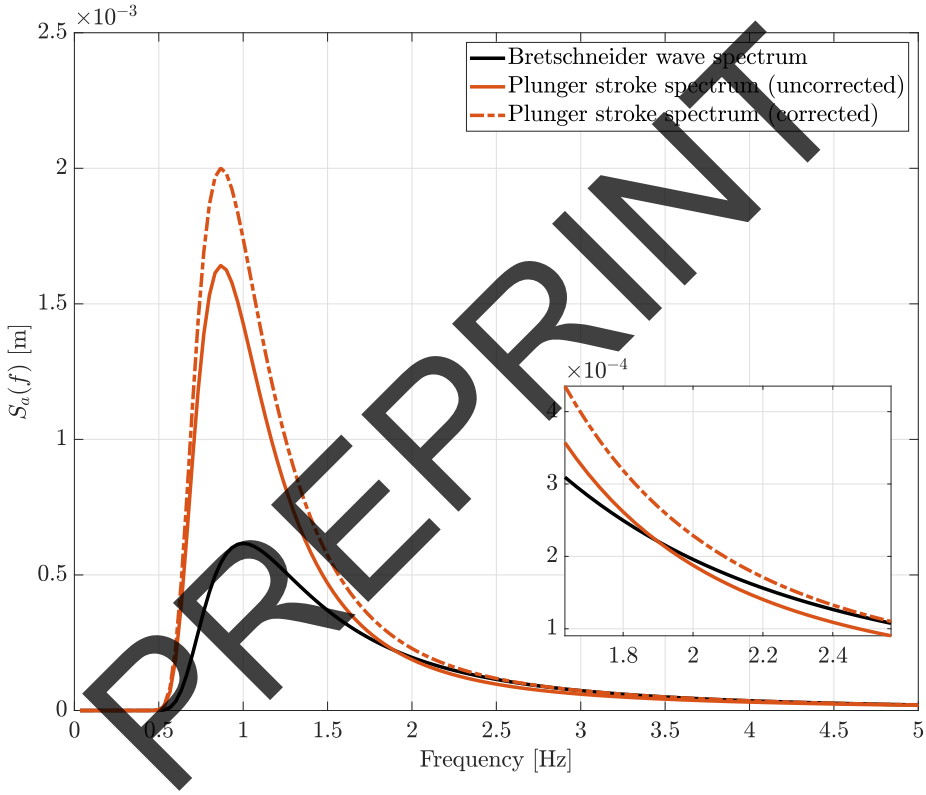

Figure 5: A comparison between the stroke amplitude spectrum of the uncorrected (solid red) and corrected (dashed red) a/s ratio for the plunger-type wavemaker as a function of frequency. The wave amplitude Bretschneider spectrum (black) is also provided.

(black) with significant wave height $H_s = 0.02$ m and peak frequency $f_0 = 1.0$ Hz is displayed along with the plunger-type wavemaker stroke amplitude spectrum without the correction (red, solid) and with the correction (red, dashed). The stroke amplitude spectra are achieved by dividing the Bretschneider wave spectrum by the value of a/s as a function of frequency. A window also displays in more detail the behaviour of each stroke spectrum between 1.7 Hz and 2.5 Hz. For the uncorrected plunger stroke spectrum, the frequency at which a/s becomes greater than one corresponds to the stroke spectrum crossing that

of the wave spectrum, exhibiting the amplification behaviour previously mentioned. Whereas, when the correction is included, the magnitude of the stroke spectrum is always greater than or equal to that of the wave spectrum such that no wave amplification will occur. It is also be noted that in general, the correction works to increase the stroke amplitude magnitude at each frequency, effectively increasing the energy in the system when generating waves. While the plunger-type transfer function more closely resembles that of the piston- and flap-types with the applied correction, it is important to also validate the correction experimentally.

4. Experimental Design

To validate both the generation of irregular waves with the given plunger-type system as well as the proposed correction to the PTF model, a series of experimental tests were conducted. The aim of each experimental test was to recreate a Bretschneider energy spectrum within the water channel given a significant wave height H_s and peak frequency f_0 that could be scaled to the real-world sea state conditions in Table 1.

For scaled model testing, it is desirable to retain the same balance between inertial, gravitational, and viscous effects as that of the full-scale phenomenon. Thus, for the wave energy applications in this paper, the dimensional scaling of the sea states is performed using Froude scaling laws [44]. The geometric scale factor between the model- and full-scale condition is represented by the scale factor λ. Following the Froude scaling laws, the model-scale significant wave height H_s is related to the full-scale significant wave height H_{s_λ} by,

$$H_s = \frac{H_{s_\lambda}}{\lambda}, \tag{12}$$

while the model-scale modal period T_p is related to the full-scale modal period T_{p_λ} by,

$$T_p = \frac{T_{p_\lambda}}{\sqrt{\lambda}}. \tag{13}$$

Therefore, by scaling the parameters of the full-scale sea states to that of the laboratory scale, a set of Bretschneider spectra were considered for experimental validation. The limitations of the plunger-system were also taken into consideration with respect to the size of the wedge and water channel.

The experimental tests were divided into an initial set which considered a larger range of significant wave height and peak frequencies and a secondary set which focused on a smaller range of parameters. Fig. 6 displays the initial (black cross) and secondary (red circle) set of tests that were conducted with respect to the significant wave height and peak frequencies used to describe each Bretschneider spectrum. The secondary test set has been labelled with numbers 1-12 for clarity in the discussion of the results. Note that tests 1, 4, 5, 8, 9, and 12 in the secondary test set were also performed in the initial test set in order

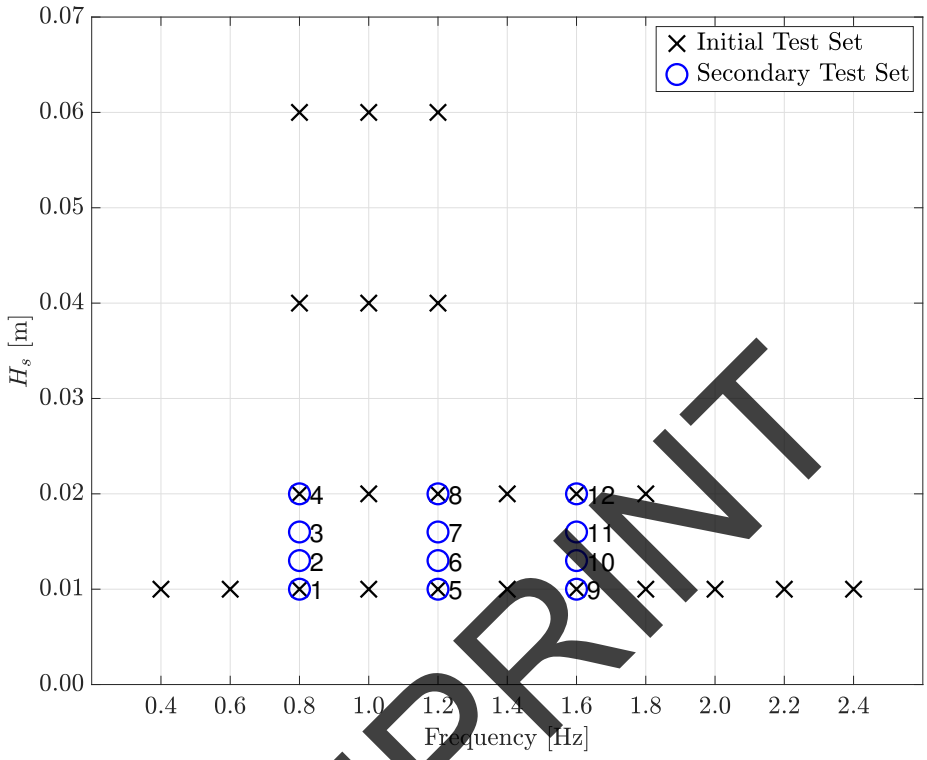

Figure 6: The significant wave height and peak frequency for each Bretschneider spectrum experimentally generated for the initial test set (black cross) and secondary test set (red circle).

to analyze the repeatability of the tests. Each energy spectrum corresponding to test parameters in Fig. 6 were also tested for the system's operational mean flows of 0.000 m/s, 0.076 m/s, 0.152 m/s, and 0.229 m/s [42]. To conduct each test, the Bretschneider energy spectrum in Eq. (3) was first determined for the chosen significant wave height and peak frequency. The spectrum was then converted to a wave amplitude spectrum using,

$$S_a(f) = \sqrt{(2S_B(f)F_s/l)}, \tag{14}$$

where F_s is the sampling rate and l is length of frequency vector. As previously mentioned, the PTF model takes in a single frequency in order to determine the transfer function a/s. Since the wave amplitude spectrum consists of a range of frequencies, the PTF model was then used to determine a value of a/s as a function of frequency, while the remaining input parameters were held constant. Dividing the wave amplitude spectrum by the frequency-dependent transfer function thus resulted in a stroke amplitude spectrum $S_s(f)$. An inverse Fast Fourier Transform was then applied to $S_s(f)$, with the inclusion of a randomly determined phase, resulting in a time domain control signal for the plunger

system $z(t)$.

The generated wave profile in the water channel was measured using a SICK ultrasonic sensor [41] with each testing running for 120 seconds. The water depth was set to 0.60 m and was taken into account prior to experimental testing as it is required for the PTF model in order to generate the desired control signal. The results of the experimental tests for both the initial and secondary sets are presented in the following section.

5. Experimental Results

The results of the experimental work are presented in the following subsections. First, the results of the experimental work when no correction is applied to the PTF model are presented with respect to the percent error in significant wave height and peak frequency. Second, the experimental results are presented with the applied correction to the PTF model including a comparison between the uncorrected and corrected results. To evaluate the results, a percent error metric was used which follows the form,

$$\% \text{ error} = \left(\frac{\text{theoretical} - \text{measured}}{\text{measured}} \right) \times 100, \tag{15}$$

where "theoretical" indicates the desired value of the studied parameter and "measured" indicates the studied parameter experimentally determined by examining the experimental energy spectrum measured by the ultrasonic sensor. Since the ultrasonic sensor measures the time series of the generated irregular waves, a Fast Fourier transform is used to convert from the time domain to the frequency domain. The peak frequency is then determined by locating the frequency at which the maximum value in the measured wave energy spectrum occurs. Meanwhile, the significant wave height is determined in the frequency domain using,

$$H_s = 4\sqrt{m_0}, \tag{16}$$

where m_0 is the variance of spectrum (or zeroth moment) and defined by [45],

$$m_0 = \int_0^\infty S_B(f)\mathrm{d}f. \tag{17}$$

Thus, the significant wave height in the frequency domain is calculated for both the desired Bretschneider energy spectrum as the theoretical value and for the experimentally determined energy spectrum as the measured value in the percent error calculation in Eq. (15).

Fig. 7 provides an example measured wave profile which corresponds to test 7 in the secondary test set (see Fig. 6) for a mean flow of 0.076 m/s. Here, the desired significant wave height H_s was 0.16 m and the desired peak frequency f_0 was 1.2 Hz. A 20 second interval from 5-25 seconds has also been provided in order to visualize the time series in more detail. Across all tested wave profiles,

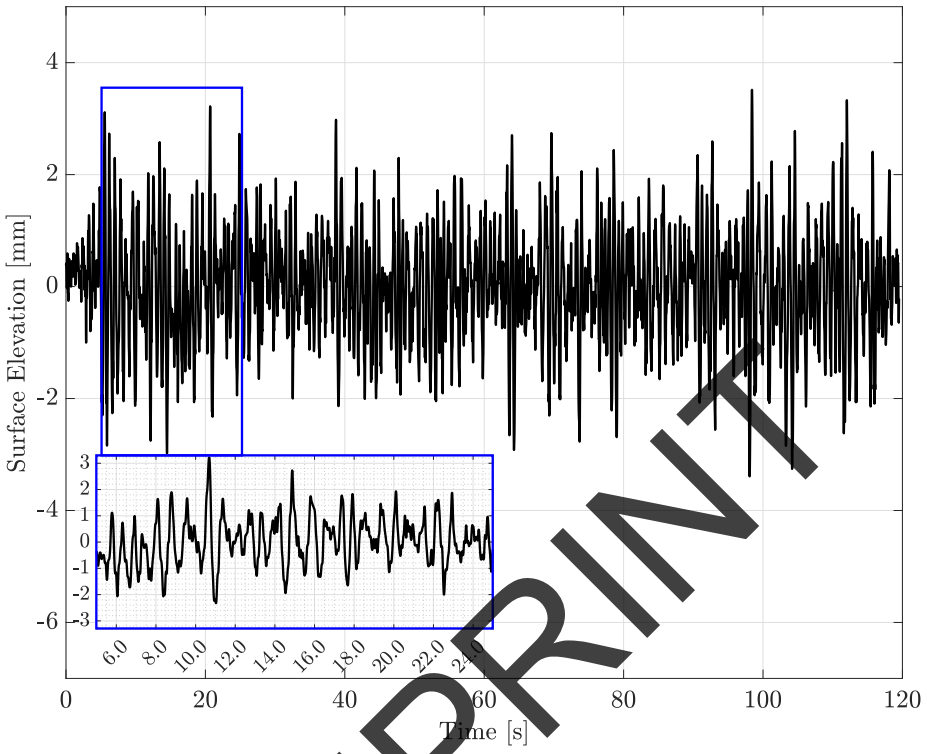

Figure 7: An example wave profile as measured by the ultrasonic sensor in the time domain. The generated wave profile corresponds to test 7 in the secondary test set for a mean flow of 0.076 m/s, such that the desired H_s was 0.16 m and f_0 was 1.2 Hz.

the number of waves generated in the measured 120 second time interval ranged from approximately 120 - 220.

To evaluate the appropriateness of the studied time interval, a statistical analysis was performed using the Kolmogorov-Smirnov (KS) test for normality at the 5% significance level [46]. The KS test was applied to the measured time series for each experimental test using the *kstest*() function within MATLAB with the associated p-value also determined. A p-value below 0.05 thus indicates the distribution is not statistically normal, on the bases that the empirical cumulative distribution function (CDF) and theoretical CDF are unequal. It was found that the majority of the experimental tests do not statistically follow a standard normal distribution. Regardless, the time series' in which $p < 0.05$ still visually follow a normal distribution and comparison of the CDFs for such tests show that there is not a considerable difference in the empirical and theoretical CDFs. For example, Fig. 8 shows a comparison of the KS test result CDFs for the best (top) and worst (bottom) p-values. Here, the best p-value occurred for test 3 (corrected) for a mean flow of 0.076 m/s, while the worst p-value occurred for test 11 (corrected) for a mean flow of 0.152 m/s. For the maximum p-value

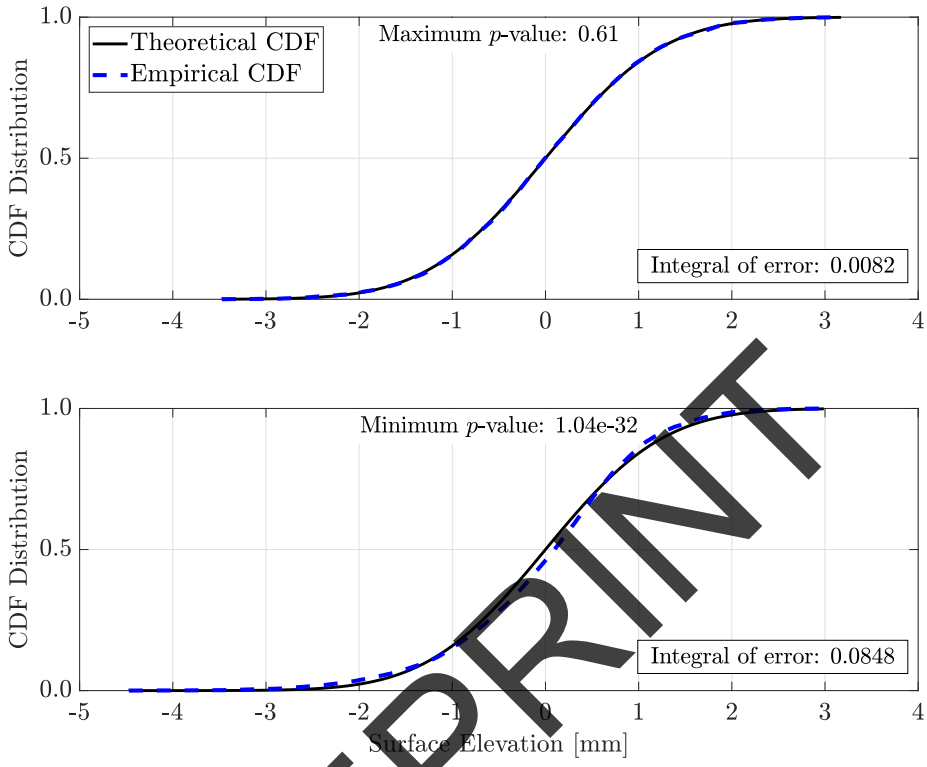

Figure 8: The results of the KS test for the best (top) and worst (bottom) p-values which occurred for corrected test 3 (0.076 m/s) and test 11 (0.152 m/s). In each plot, the empirical CDF (blue dash) is shown in comparison to the theoretical plot (black solid) along with the associated integral of error.

of 0.61, the time series is statistically determined to have a standard normal distribution with the empirical and theoretical CDFs equal to one another. On the other hand, the smallest p-value was 1.04e-32, indicating the distribution is not statistically normal; however, from Fig. 8 (bottom) the empirical CDF is still similar to the theoretical CDF despite the low p-value. Quantifying the integral of error, there is only one order of magnitude difference between each case where the integral of error for the maximum and minimum p-value was 0.0082 and 0.848, respectively. Further investigation into the rejection of the normal distribution for the experimental irregular wave profiles is thus an avenue for future research, the results of which may improve the experimental design of the research. As such, following the typical reporting for irregular wave profiles as in [10, 11, 15, 16], along with preliminary statistical analysis, the current research focuses on analyzing the percent error determined with respect to the significant wave height and peak frequency of the generated spectra.

5.1. Initial Uncorrected Results

The initial set of experimental tests are outlined in Fig. 6 (left) and consider Bretschneider spectra that incorporate a wide range of significant wave heights H_s and peak frequencies f_0 for the experimental system in consideration. Fig. 9 presents the percent error in the peak frequency for the initial set of tests as a function of the theoretical peak frequency for each Bretschneider spectra. The results in Fig. 9 are also displayed as function of mean flow in order to

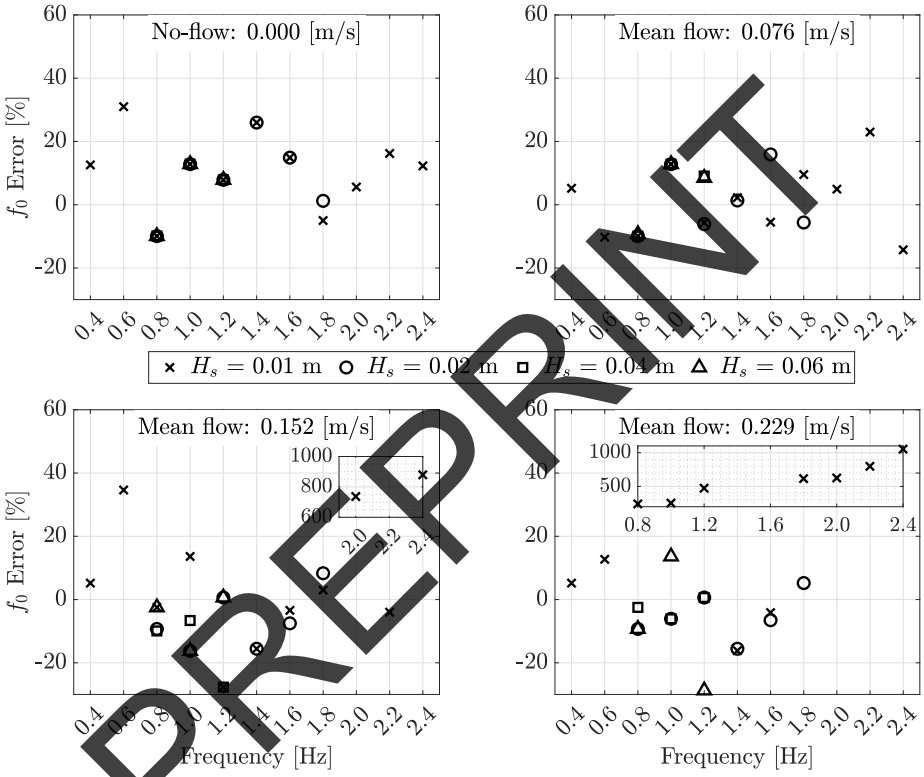

Figure 9: The percent error in the peak frequency f_0 as a function of frequency and mean flow for the set of theoretically tested wave heights on the initial set of tests without correction to the PTF model.

study the impact due the inclusion of mean flow. While there is no trend in the percent error for the peak frequency with respect to the tested value of H_s, there is an impact due to the inclusion and subsequent increase in mean flow value. For the no-flow case, the f_0 % error is similar regardless of the corresponding value of H_s; however, when a mean flow of 0.076 m/s is included, the high frequency tests for H_s equal to 0.01 m increases significantly in error. As the flow is increased further, more tests at $H_s = 0.01$ m show similarly large errors for the highest mean flow of 0.229 m/s. Since the large discrepancy between the desired and measured peak frequency occurs for the lower values of significant

wave height, the error can be attributed to the signal-to-noise ratio (SNR) due to the higher turbulence in the water channel as the mean flow increases in magnitude. In addition, although the wave absorber works to attenuate the incident wave energy, there still exists some reflected wave energy within the test section of the channel. Interference between reflected and incident waves may introduce undesired frequencies in the spectra; therefore, reflection in the channel is considered a source of error.

The percent error in the significant wave height was also considered as a metric of assessing the ability for the plunger system to generate irregular waves. Fig. 10 presents the results of the H_s % error as a function of the tested peak frequencies and mean flows. The markers represent the different theoretical

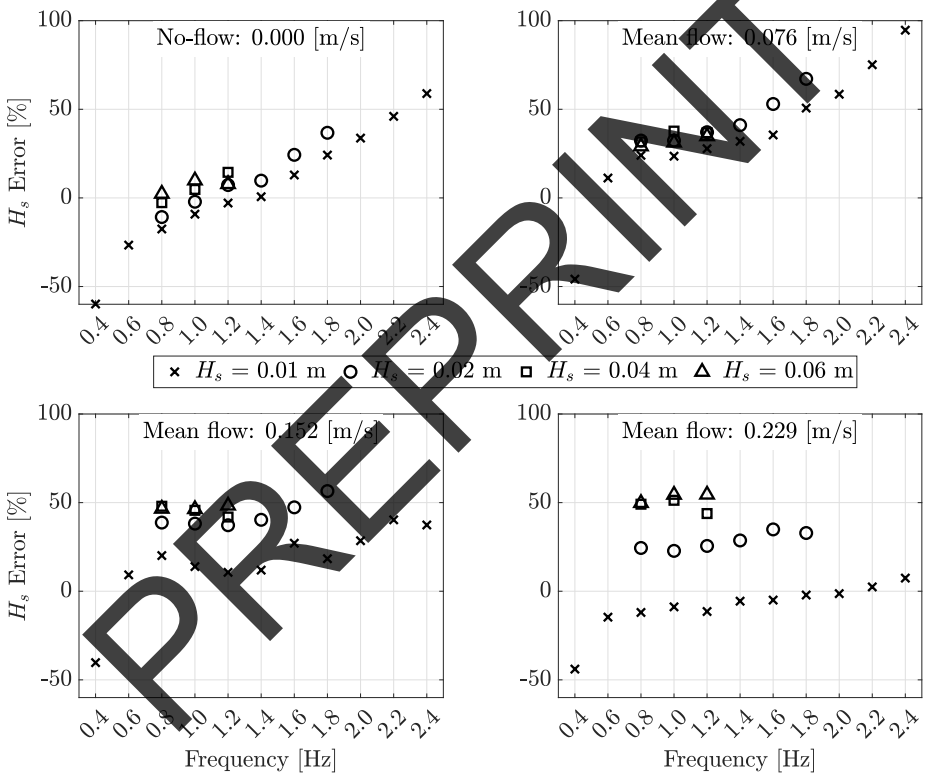

Figure 10: The percent error in the significant wave height H_s as a function of frequency and mean flow for the set of theoretically tested wave heights on the initial set of tests without correction to the PTF model.

significant wave heights tested with a negative error indicating that the experimentally produced spectrum has a larger significant wave height than the desired spectrum. Overall, the majority of tests have a positive percent error in that the generated spectrum has a lower significant wave height than the theoretically desired value. Since the significant wave height in the frequency domain is directly related to the integral of the energy spectrum, a lower sig-

nificant wave height indicates less energy in the waves. As such, the results of Fig. 10 indicate that there is a loss of energy in the system when generating the irregular spectra that may be compensated for by applying the proposed correction to the PTF transfer function.

In the no-flow case, for H_s equal to 0.01 m and 0.02 m, the percent error is lowest for intermediate frequencies with an increase in the absolute percent error as the tested frequency changes in either direction. For higher significant wave heights, the percent error is lowest for the 0.8 Hz, with an increase in error proportional to the increase in frequency. When flow is included, the results of H_s equal to 0.02, 0.04, and 0.06 m do not vary as the mean flow increases. Hence, mean flow can be included in the water channel for these tests without consequence to the accuracy of the generated irregular waves. However, there is fluctuation in the results for the 0.01 m tests. For mean flows of 0.076 m/s and 0.152 m/s, the percent error at each tested peak frequency is similar, with lower peak frequencies starting at 0.6 Hz being more accurate than higher frequencies. On the other hand, for a mean flow of 0.229 m/s, a higher peak frequencies results in lower percent errors instead. Note that regardless of the mean flow value, the spectrum with $H_s = 0.01$ m and $f_0 = 0.4$ Hz is always the least accurate; a result which may be due to a poor SNR, especially for the higher mean flows. Therefore, a combination of $H_s = 0.01$ m and $f_0 = 0.4$ Hz is not an appropriate choice of parameters for creating irregular waves for this system. Error in the results may also be a result of hydrodynamic phenomena within that channel that are not fully taken into account such as reflection and leakage around the wedge. Additionally, there is a gap which grows between the 0.01 m tests and the remaining tests as the magnitude of the mean flow increases. To understand the reasoning for the apparent gap, spectra with intermediate peak frequencies and significant wave heights between 0.01 m and 0.02 m are studied in the following section along with validation of the proposed correction to the PTF model.

5.2. Secondary Uncorrected and Corrected Results

The spectrum parameters for the secondary set of tests are shown in Fig. 6 (red circles) and include a repetition of significant wave heights 0.01 m and 0.02 m with additional intermediate significant wave heights of 0.013 m and 0.016 m. Fig. 11 displays the percent error in the peak frequency f_0 for the secondary set of tests as a function of the theoretical peak frequency. Note that the markers for $H_s = 0.01$ m (x) and $H_s = 0.02$ m (o) are the same as those used in Fig. 9 in order to directly compare the results. The impact of flow on the percent error in the secondary tests follows a similar trend as those in the initial test set. As the magnitude of mean flow increases, there is a large positive percent error with results from the H_s equal to 0.01 m for mean flows of 0.152 m/s and 0.229 m/s. In addition, the magnitude of error in the peak frequency for the tests common to both the initial and secondary test sets are comparable for assessing the repeatability of the generated irregular wave spectra. Table 2 summarizes the absolute difference in percent error between initial and secondary tests that had the same input parameters. The majority of the tests that were repeated

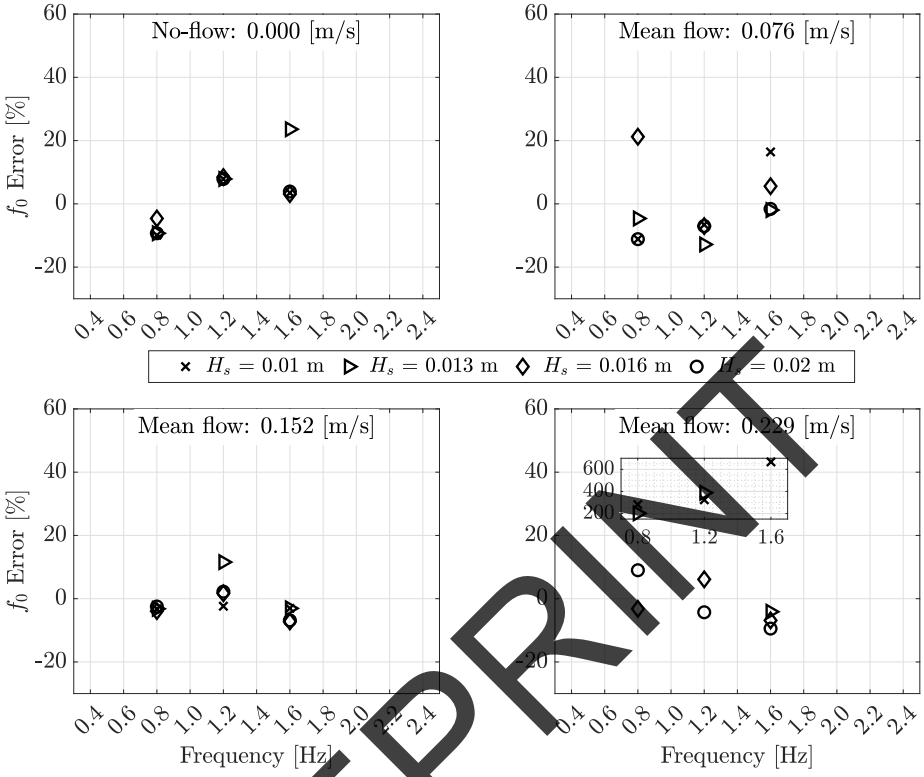

Figure 11: The percent error in the peak frequency f_0 as a function of frequency and mean flow for the set of theoretically tested wave heights on the secondary set of tests without correction to the PTF model.

had differences in the percent error under 5%. Larger differences in the error are mostly observed for the peak frequency at high flow rates, specifically test 5 and 9 for 0.229 m/s mean flow, where the increased water turbulence may cause underlying frequencies in the spectra that are undesired and shift the measured peak frequency. As such, these higher mean flows present the upper operational bounds of the system under study. That said, with respect to the significant wave height, the low differences in percent error regardless of mean flow indicate that the generated spectra are repeatable with respect to the wave energy.

Similarly, Fig. 12 displays the significant wave height percent error for the secondary set of tests separated by the no-flow and mean flow cases. As with the secondary peak frequency results, the markers for $H_s = 0.01$ m (x) and $H_s = 0.02$ m (o) have been repeated from Fig. 10. Comparing the initial test results in Fig. 10 and secondary test results in Fig. 12, the percent errors in the 0.01 m and 0.02 m tests are of similar magnitude for both the no-flow and mean flow cases, reinforcing the repeatability of generating irregular waves with the given system. With regard to the significant wave heights of 0.013 m and 0.016 m in the no-flow case, the percent error magnitude is similar to the other tested

Table 2: Absolute difference in percent error between initial and secondary tests.

	Test No.	1	4	5	8	9	12
f_0	0.000 m/s	0.00	0.63	0.00	0.00	11.40	10.98
	0.076 m/s	1.23	1.23	0.90	0.89	21.93	17.49
	0.152 m/s	0.73	6.82	25.31	1.58	0.36	0.66
	0.229 m/s	40.16	18.29	149.80	4.93	671.12	2.92
H_s	0.000 m/s	3.91	5.00	2.65	0.75	3.07	3.08
	0.076 m/s	1.75	0.89	0.50	2.82	12.73	8.33
	0.152 m/s	3.33	1.39	3.76	1.40	5.74	1.21
	0.229 m/s	0.97	3.41	0.00	0.19	10.99	1.72

values of H_s. As mean flow is included, the magnitude of the percent error addresses the gap that was observed in the respective mean flow cases in Fig. 10. Thus, for a mean flow of 0.152 m/s, as the significant wave height increases from 0.01 m to 0.02 m, the percent error also increases. On the other hand, for the highest mean flow, the percent error approaches zero before increasing again with an increase in significant wave height.

As in Fig. 10, the majority of the secondary tests have a positive percent error such that the energy in the observed spectra is less than the desired amount. From Fig. 5, it was shown that the correction to the PTF model's transfer functions works to increase the energy in the spectrum while the peak frequency remains the same. Therefore, for the same desired values of significant wave height and peak frequency for a given spectrum, the generated irregular waves will theoretically have a larger significant wave height when the correction is included. To validate the proposed correction, the secondary set of tests were repeated but with first correcting a/s as a function of frequency for the plunger system before determining the correspond time-domain control signal. Fig. 13 shows a side-by-side comparison of the significant wave height percent error for each of the twelve secondary tests without the correction (blue) and with the correction (red). For each of the tests, the correction has increased the energy in the generated waves, consequently increasing the measured significant wave height in the frequency domain. Hence, for the uncorrected results in Fig. 13 which had a positive percent error for H_s, the corrected results are more close in magnitude to the theoretical significant wave height, resulting in a lower percent error. However, in some cases, such as tests 6-9 in the no-flow case, the increase in error has caused an overshoot in the significant wave height, leading to negative percent errors that were previously positive. Furthermore, uncorrected tests in which the measured significant wave height is larger than the desired value, which includes tests 1-4 for the no-flow case and tests 1, 2,

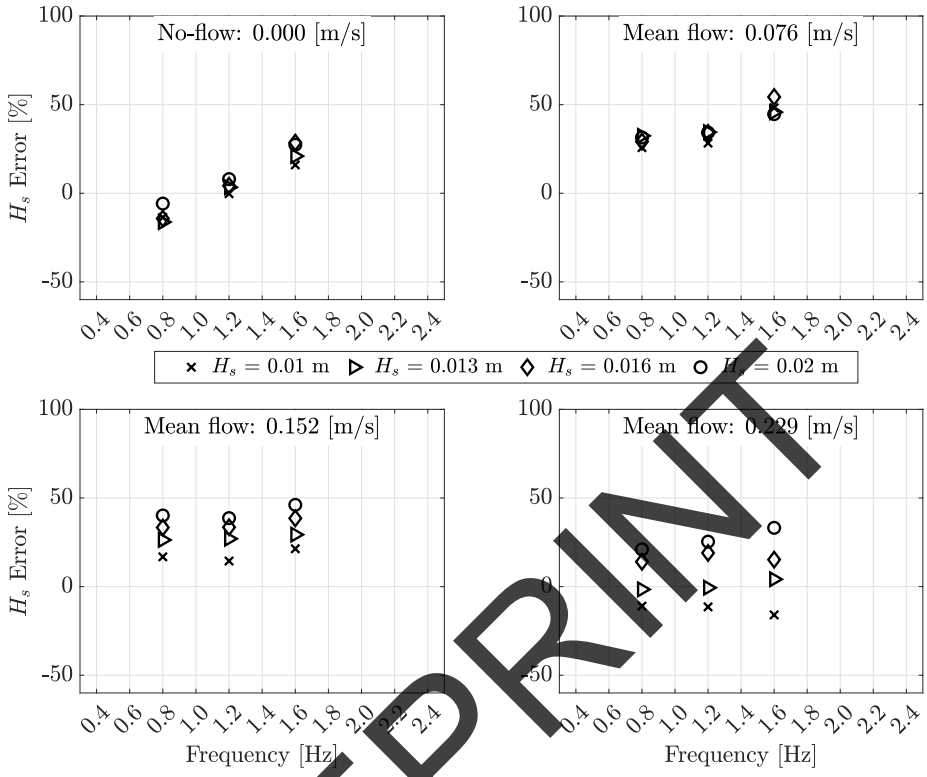

Figure 12: The percent error in the significant wave height H_s as a function of frequency and mean flow for the set of theoretically tested wave heights on the secondary set of tests without correction to the PTF model.

5, 6, and 9 for a mean flow of 0.229 m/s, corresponds to a negative percent error. The cause for higher energy in these tests than desired may be due to the poor SNR between the generated wave signal and noise due to turbulence in the channel which can include reflected wave energy and mean flow. In particular, tests 1, 5, and 9 correspond to the lowest significant wave height tested of 0.01 m meaning that on average two-thirds of the waves have heights lower than 0.01 m. Thus, these signals may be difficult to measure in comparison to the energy due to various hydrodynamic phenomena within the channel. For uncorrected and corrected test, the SNR was quantified by comparing the measured wave signal to a measurement of the water when no waves are generated. In doing so, it was determined that the highest SNR was 8.27 corresponding to test 4 (corrected) in the no-flow case. Meanwhile, the poorest SNR was 0.98, corresponding to test 1 (uncorrected) in the 0.229 m/s flow case, the result of which is not unexpected as test 1 has the lowest significant wave height accompanied by the highest mean flow, representing the limit of the system. The tests with low percent error in both the significant wave height and peak frequency also showed high SNRs, for example, test 8 (corrected) in the no-flow case had a SNR of 6.18, while test

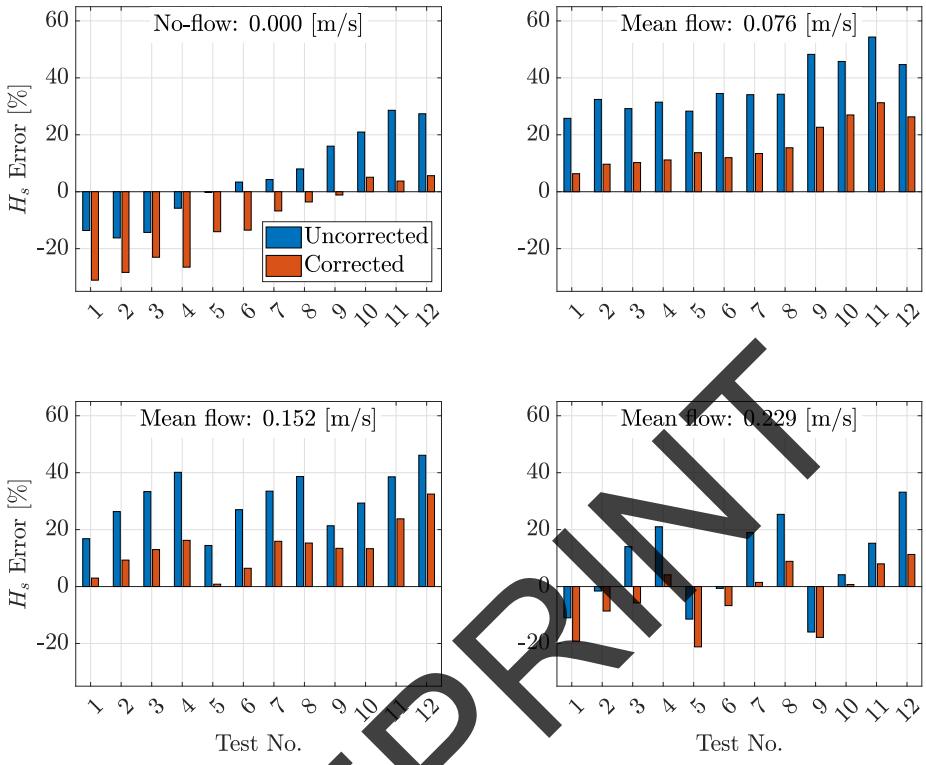

Figure 13: A comparison between the uncorrected (blue) and corrected (red) percent error in the significant wave height H_s.

2 (corrected) for 0.076 m/s had a SNR of 4.12. Regardless, for the majority of tests, the correction to the PTF model has decreased the absolute percent error in the significant wave height; therefore, the proposed correction is valid, especially when low mean flow is included in the water channel.

To study the impact of the model correction on the peak frequency, Fig. 14 displays the comparison in the peak frequency percent error for each of the secondary tests without the correction (blue) and with the correction (red). For the majority of the considered tests, the effect of the correction to a/s was minor; however, such a result is expected since the correction did not affect the peak frequency of the control signal. That being said, there are some cases in which a change in the peak frequency is observed. Most notable is for test 2 and test 9 for a mean flow of 0.229 m/s wherein the correction eliminated the substantial error in the peak frequency. Since the peak frequency was determined by finding the local maxima in the spectra, the increase in energy due to the correction may have caused a peak more closely to that of the desired peak frequency to become more prominent. On the other hand, there were tests wherein the absolute percent error of the peak frequency increased, such as test 1, no flow and tests 5 and 8 for a mean flow of 0.152 m/s. The increase in error for the no-flow

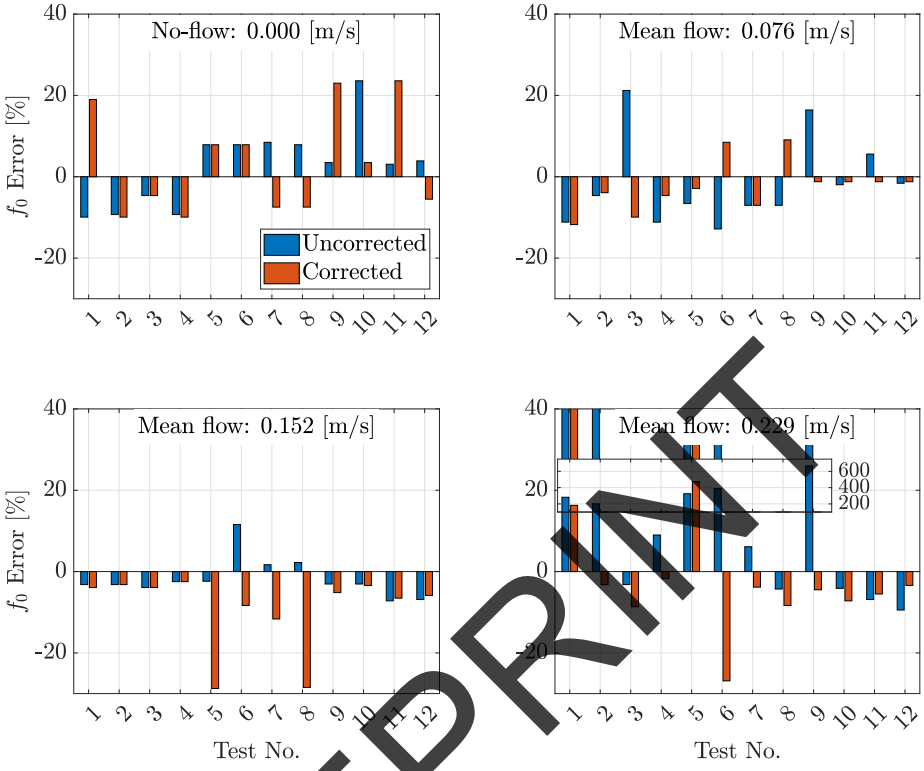

Figure 14: A comparison between the uncorrected (blue) and corrected (red) percent error in the peak frequency f_0.

cases may be due to the small amplitudes of the generated waves. Meanwhile, the inclusion of mean flow along with the small amplitude waves may lead to a poor SNR causing an undesired shift in the peak frequency of the spectrum. In quantifying the SNR, it was found that as expected, the highest mean flow often has a poorer ratio. That said, the no-flow case also produced poor SNRs for small amplitude waves. For example, test 9 (corrected) in the no-flow case had a SNR of 2.62 in comparison to the maximum SNR of 8.27 which occurred for test 4 (uncorrected) in the no-flow case. Therefore, in general, the proposed correction is valid with respect to the peak frequency; however, improvements to either the system or theory are still required in order to alleviate the large errors, especially at higher mean flows.

6. Conclusion

An experimental validation of generating irregular waves for both mean flow and no-flow cases using a plunger-type wavemaker has been studied with validation of the inclusion of a correction to the plunger-type flow (PTF) model. To

generate irregular waves in a laboratory water channel that resemble scaled versions of the Bretschneider spectrum, the transfer function between a wavemaker and the water must be considered for the range of frequencies of which the desired spectrum is comprised. It was shown that when compared to the transfer functions of piston- and flap-type wavemakers, the transfer function for plunger-type wavemakers differs significantly in that it suggests implausible wave amplification, nor does it saturate as frequency is increased. As such, a correction to the PTF model which limits a/s to a maximum of one before saturating the function was proposed. The proposed correction was subsequently validated through experimental testing of a plunger-type wavemaker system. The ability for the wavemaker to create irregular waves was first studied through a initial set of experimental tests which showed that peak frequency could be well predicted at no-flow or low mean flow cases but, as the mean flow increased there were large errors for spectra who had smaller significant wave heights. Similarly, the initial test results showed that in general, lower or intermediate peak frequencies lead to more accurately predicted significant wave heights. A secondary set of tests, which focused on a smaller range of significant wave height and peak frequencies in irregular wave spectra, was then presented which addressed gaps in percent error that were observed in the initial tests. In addition, the secondary set of tests were used to directly compare the spectra generated with and without the correction applied to the PTF model. The direct comparison exemplified the necessity of the correction, especially when mean flow is included in the water channel. Therefore, with the addition of the correction to the PTF model, plunger-type wavemakers are a valid tool for generating irregular waves in a laboratory setting for both mean flow and no-flow scenarios.

Acknowledgements

The authors acknowledge the support of the Natural Sciences and Engineering Research Council of Canada (NSERC), [funding reference numbers RGPIN-2017-06967, RGPIN-2022-04934]. Cette recherche a été financée par le Conseil de recherches en sciences naturelles et en génie du Canada (CRSNG), [numéros de référence RGPIN-2017-06967, RGPIN-2022-04934]. Additionally, we would like to acknowledge Mitacs as support for the work was maintained through a Research Training Award (RTA) [reference number IT#19361], Kraken Robotic Systems Inc. for their support with the hardware development, and Carleton University for the equipment infrastructure.

References

[1] U. D. Nielsen, R. E. Mounet, A. H. Brodtkorb, Tuning of transfer functions for analysis of wave–ship interactions, Marine Structures 79 (2021) 103029. doi:https://doi.org/10.1016/j.marstruc.2021.103029.

[2] Y. Luo, C. Zhang, J. Liu, H. Xing, F. Zhou, D. Wang, X. Long, S. Wang, W. Wang, F. Shi, Identifying ship-wakes in a shallow estuary using machine

learning, Ocean Eng. 246 (2022) 110456. doi:https://doi.org/10.1016/j.oceaneng.2021.110456.

[3] W. Lyu, O. el Moctar, T. E. Schellin, Ship motion-sloshing interaction with forward speed in oblique waves, Ocean Eng. 250 (2022) 110999. doi:https://doi.org/10.1016/j.oceaneng.2022.110999.

[4] R. Irani, W. Spencer, Future launch and recovery system, in: American Society of Naval Engineers: Launch & Recovery of Manned and Unmanned Vehicles from Surface Platforms, Linthicum, Maryland, 2014.

[5] C. Calnan, R. Bauer, R. Irani, Reference-point algorithms for active motion compensation of towed bodies, IEEE J. Ocean. Eng. 44 (4) (2018) 1024–1040. doi:10.1109/JOE.2018.2866317.

[6] C. Westin, R. Irani, Modelling dynamic cable-sheave contact and detachment during towing operations, Marine Structures 77 (2021) 102960. doi:https://doi.org/10.1016/j.marstruc.2021.102960.

[7] E. Chappell, Theory and design of a wave generator for a short flume, MASc, University of British Columbia, Vancouver, British Columbia (1969).

[8] S. Lowell, J. McPhee, R. Irani, Plunger-type wavemakers with flow: Sensitivity analysis and experimental validation, Appl. Ocean Res. 121 (2022) 103065. doi:https://doi.org/10.1016/j.apor.2022.103065.

[9] I. Miskovic, Z. Eskinja, K. Horvat, Wavemaker control system for irregular developed sea waves generation, in: 2008 16th Mediterranean Conference on Control and Automation, 2008, pp. 791–794. doi:10.1109/MED.2008.4602205.

[10] C. Raoult, M. Benoit, M. Yates, Validation of a fully nonlinear and dispersive wave model with laboratory non-breaking experiments, Coastal Eng. 114 (2016) 194–207. doi:https://doi.org/10.1016/j.coastaleng.2016.04.003.

[11] L. Riefolo, P. Contestabile, F. Dentale, G. Benassai, Low frequency waves detected in a large wave flume under irregular waves with different grouping factor and combination of regular waves, water 10 (2). doi:https://doi.org/10.3390/w10020228.

[12] A. Khait, L. Shemer, Nonlinear wave generation by a wavemaker in deep to intermediate water depth, Ocean Eng. 182 (2019) 222–234. doi:https://doi.org/10.1016/j.oceaneng.2019.04.065.

[13] G. Xu, H. Hao, Q. Ma, Q. Gui, An experimental study of focusing wave generation with improved wave amplitude spectra, water 11 (2019) 2521. doi:https://doi.org/10.3390/w11122521.

[14] H. G. Guler, B. E. Larsen, O. Quintana, K. D. Goral, S. Carstensen, E. D. Christensen, N. B. Kerpen, T. Schlurmann, D. R. Fuhrman, Experimental study of non-buoyant microplastic transport beneath breaking irregular waves on a live sediment bed, Marine Pollution Bulletin 181 (2022) 113902. doi:https://doi.org/10.1016/j.marpolbul.2022.113902.

[15] M. Hasnan, H. Yasukawa, N. Hirata, D. Terada, A. Matsuda, Study of ship turning in irregular waves, J. Mar. Sci. Technol. 25 (2020) 1024–1043. doi:https://doi.org/10.1007/s00773-019-00698-1.

[16] B. Sun, C. Li, S. Yang, H. Zhang, A simplified method and numerical simulation for wedge-shaped plunger wavemaker, Ocean Eng. 241 (2021) 110023. doi:https://doi.org/10.1016/j.oceaneng.2021.110023.

[17] F. Ursell, On the heaving motion of a circular cylinder on the surface of a fluid, Q. J. Mech. Appl. Math. 2 (2) (1949) 218–231. doi:https://doi.org/10.1093/qjmam/2.2.218.

[18] F. Ursell, Water waves generated by oscillating bodies, Q. J. Mech. Appl. Math. 7 (4) (1954) 427–437. doi:https://doi.org/10.1093/qjmam/7.4.427.

[19] Y. Yu, F. Ursell, Surface waves generated by an oscillating circular cylinder on water of finite depth: theory and experiment, J. Fluid Mech. 11 (1961) 529–551. doi:https://doi.org/10.1017/S0022112061000718.

[20] S. Wang, Plunger-type wavemakers: theory and experiment, J. Hydraul. Res. 127 (3) (1974) 357–388. doi:https://doi.org/10.1080/00221687409499732.

[21] F. Biesel, Laboratory wave-generating apparatus, in: English translation in Project Report No. 39, M. Pilch, St. Anthony Falls Hydraulic Laboratory, Univ. of Minnesota, Minneapolis, Minn., 1953. doi:https://hdl.handle.net/11299/108277.

[22] J. Hyun, Simplified analysis of a plunger-type wavemaker performance, J. Hydronautics 10 (3) (1976) 89–94. doi:https://doi.org/10.2514/3.63056.

[23] D. Ellix, K. Arumugam, An experimental study of waves genereated by an oscillating wedge, J. Hydraul. Res. 22 (5) (1984) 299–313. doi:https://doi.org/10.1080/00221688409499367.

[24] M. Kashiwagi, Full-nonlinear simulations of hydrodynamics forces on a heaving two-dimensional body, J. Society of Naval Architects of Japan 180 (1996) 373–381. doi:https://doi.org/10.2534/jjasnaoe1968.1996.180_373.

[25] T. Mikkola, Time accurate simulation of a plunger type wave maker using unstructured finite volume solver with surface tracking, in: 26th Symposium on Naval Hydrodynamics, Rome, Italy, 2006.

[26] T. Mikkola, Simulation of plunger-type wavemakers, J. Structural Mechanics 40 (4) (2007) 19–39.

[27] M. He, A. Khayyer, X. Gao, W. Xu, B. Liu, Theoretical method for generating solitary waves using plunger-type wavemakers and its smoothed particle hydrodynamics validation, Appl. Ocean Res. 106 (2021) 102414. doi:https://doi.org/10.1016/j.apor.2020.102414.

[28] Y.-C. Wu, Plunger-type wavemaker theory, J. Hydraul. Res. 26 (4) (1988) 483–491. doi:https://doi.org/10.1080/00221688809499206.

[29] Y.-C. Wu, Waves generated by a plunger-type wavemaker, J. Hydraul. Res. 29 (6) (1991) 851–860. doi:https://doi.org/10.1080/00221689109498963.

[30] J. Gadelho, A. Lavrov, C. G. Soares, R. Urbina, M. Cameron, K. Thiagarajan, CFD modelling of the waves generated by a wedge-shaped wave maker, in: C. G. Soares, T. Santos (Eds.), Maritime Technology and Engineering, Taylor & Francis Group, 2015, pp. 993–1000.

[31] Z. Azadian-Kharanjani, A. Nikseresht, H. Bingham, A numerical investigation of wedge angle effects on a plunger type wave maker with a constant submerged volume, in: ASME 2018 37th International Conference on Ocean, Offshore and Arctic Engineering, Madrid, Spain, 2018. doi:https://doi.org/10.1115/OMAE2018-77380.

[32] A. Nikseresht, H. Bingham, A numerical investigation of gap and shape effects on a 2d plunger-type wave maker, J. Mar. Sci. and App. 19 (2020) 101–115. doi:https://doi.org/10.1007/s11804-020-00135-5.

[33] S. Lowell, R. Irani, Sensitivity analysis of plunger-type wavemakers with water current, in: IEEE Global OCEANS 2020:Singapore - U.S. Gulf Coast, Virtual, 2020.

[34] J. Hicks, H. Bingham, R. Read, A. Engsig-Karup, Nonlinear wave generation using a heaving wedge, Appl. Ocean Res. 108 (2021) 102540. doi:https://doi.org/10.1016/j.apor.2021.102540.

[35] A. Boon, P. Wellens, Probability and distribution of green water events and pressures, Ocean Eng. 264 (2022) 112429. doi:https://doi.org/10.1016/j.oceaneng.2022.112429.

[36] N. A. T. O. (NATO), NATO - STANAG 4194 Standardized Wave and Wind Environments and Shipboard Reporting of Sea Conditions, North Atlantic Treaty Organization, 1983.

[37] R. Stewert, Introduction to Physical Oceanography, Texas A & M University, 2008.

[38] K. McTaggart, ShipMo3D Version 3.0 user manual for computing ship motions in the time and frequency domains, DRDC Atlantic TM 2011-308, 2011.

[39] S. Chakrabarti, Handbook of Offshore Engineering, Elsevier, 2008.

[40] R. Dean, R. Dalrymple, Water Wave Mechanics for Engineers and Scientists, World Scientific, 1991.

[41] SICK, UM18-218126111 Product data sheet (2022).
URL https://cdn.sick.com/media/pdf/7/67/767/dataSheet_UM18-218126111_6048404_en.pdf

[42] S. Lowell, Sensitivity analysis and experimental validation of plunger-type wavemakers modelled with a steady flow, MASc, Carleton University, Ottawa, Ontario (2021).

[43] J. McPhee, Control, simulation, and testbed development for improving maritime launch and recovery operations, MASc, Carleton University, Ottawa, Ontario (2019).

[44] G. Payne, Guidance for the experimental tank testing of wave energy converters, SuperGen Marine, 2008.

[45] Y. Bai, W. Jin, Marine Structural Design, Butterworth Heinemann, 2015.

[46] R. H. C. Lopes, Kolmogorov-Smirnov Test, Springer, Berlin, Heidelberg, 2011, pp. 718–720. doi:10.1007/978-3-642-04898-2_326.